APCTP Pre2020-019
BONN-TH-2020-07

R-parity Violation and Light Neutralinos at ANUBIS and MAPP

Herbert K. Dreiner,[1,*] Julian Y. Günther,[1,†] and Zeren Simon Wang[2,3,‡]

[1] *Bethe Center for Theoretical Physics & Physikalisches Institut der Universität Bonn, Nußallee 12, 53115 Bonn, Germany*

[2] *Department of Physics, National Tsing Hua University, Hsinchu 300, Taiwan*

[3] *Asia Pacific Center for Theoretical Physics (APCTP) - Headquarters San 31, Hyoja-dong, Nam-gu, Pohang 790-784, Korea*

In R-parity-violating supersymmetry the lightest neutralino can be very light, even massless. For masses in the range 500 MeV $\lesssim m_{\tilde{\chi}_1^0} \lesssim$ 4.5 GeV the neutralino can be produced in hadron collisions from rare meson decays via an R-parity violating coupling, and subsequently decay to a lighter meson and a charged lepton. Due to the small neutralino mass and for small R-parity violating coupling the lightest neutralino is long-lived, leading to displaced vertices at fixed-target and collider experiments. In this work, we study such signatures at the proposed experiments ANUBIS and MoEDAL-MAPP at the LHC. We also compare their sensitivity reach in these scenarios with that of other present and proposed experiments at the LHC such as ATLAS, CODEX-b, and MATHUSLA. We find that ANUBIS and MAPP can show complementary or superior sensitivity.

arXiv:2008.07539v2 [hep-ph] 19 Mar 2021

I. INTRODUCTION

Recently there has been an increased interest in long-lived particles (LLPs). Such particles are defined at colliders to have detached vertices (DVs). Instead of promptly decaying after production, they travel for a macroscopic distance before decaying within the detector, or in nearby additional detectors. Such a long lifetime can arise for different reasons such as small mass splitting, feeble couplings, or a heavy mediator. While LLPs exist already in the Standard Model (SM), such as the long-lived hadron K_L, they are also frequently predicted in a variety of BSM models motivated by either dark matter or the non-vanishing neutrino masses. For example, portal-physics models connecting the SM and dark sectors may lead to such LLPs which have a tiny coupling with the SM particles. These models may include dark photons (vector portal), a light scalar (Higgs portal), axion-like particles (pseudoscalar portal), or heavy neutral leptons (fermion portal). Moreover, other theoretical scenarios such as quirky models and split supersymmetry (SUSY) models also predict LLPs. For recent reviews of LLP models and studies, see Refs. [1–3].

We are here interested in supersymmetric models with light neutralinos. Searches for promptly decaying heavy supersymmetric fields have been unsuccessful so far. Lower limits on the masses of squarks and gluinos have been placed at the order of TeV in various SUSY models. However, this is not the case for the lightest neutralino, $\tilde{\chi}_1^0$. It was noticed some time ago [4, 5], that if we drop the GUT (grand unified theory) motivated relation of the gaugino masses $M_1 = \frac{5}{3}\tan^2\theta_W M_2$ and drop the dark matter constraint on the lightest neutralino [6–11], then the neutralino mass can be below a GeV and even massless [12, 13]. Such a light neutralino is consistent with stellar cooling, of supernovæ [14–17], and of white dwarfs [18], as well as with cosmology [19, 20]. Such light neutralinos, if stable, result in a relic energy density overclosing the Universe [21]. Thus they must decay. In R-parity violating supersymmetry (RPV-SUSY) models, see Refs. [22–24] for reviews, the lightest neutralino decays via the RPV couplings. When both the mass of the lightest neutralino and the RPV couplings are sufficiently small, the lightest neutralino is long-lived.

Searches for light long-lived neutralinos have been studied in various experimental setups. These include existing fixed-target experiments [5, 25–27], a proposed new fixed-target experiment: `SHiP` at CERN [28–30], the `ATLAS` experiment [30] and a variety of proposed dedicated experiments at the LHC: `CODEX-b` [31, 32], `FASER` [33–35], `MATHUSLA` [3, 36], and `AL3X` [37]) [38–40], and future $Z-$factories [41, 42].[1] In this work, we consider two relatively new proposals of dedicated experiments for searching for neutral LLPs at the LHC,

* dreiner@uni-bonn.de
† s6juguen@uni-bonn.de
‡ wzs@mx.nthu.edu.tw

[1] Both `ATLAS` and `CMS` have searched for heavier long-lived neutralinos. The hadronic decays are then to jets instead of light mesons, as we consider here. See for example Refs. [43, 44] and references therein.

namely ANUBIS ("An Underground Belayed In-Shaft experiment") [45, 46] and MAPP ("MoEDAL Apparatus for the detection of Penetrating Particles") [47]. ANUBIS is to consist of a cylindrical detector installed inside one of the service shafts above either the ATLAS or CMS interaction point (IP), with an expected integrated luminosity of 3 ab^{-1}. MAPP is planned with two phases and to be installed inside the UGCI gallery near the interaction point 8 (IP8) of the LHC, where the experiment LHCb is located. MAPP1 and MAPP2 are projected to have an integrated luminosity of 30 and 300 fb^{-1}, respectively. The details of these three experiments are discussed in Sec. III.

In the existing literature on the search for long-lived light neutralinos at various experiments, two types of production mechanisms have been considered. The first is rare $Z-$boson decays into a pair of the lightest neutralinos via the small Higgsino component [38, 40–42, 48], and the second is rare meson decays into a single neutralino plus a neutral or charged lepton via an RPV coupling [5, 25–27, 30, 39, 40]. In this work, we focus on the long-lived light neutralinos in RPV-SUSY, produced from a rare charm or bottom meson decay. The neutralino decays via an RPV coupling, again to a meson and a lepton. Taking one benchmark scenario for charmed and bottomed mesons, respectively, we compare the sensitivity reach of ANUBIS and MAPP experiments with other present and proposed experiments at the LHC.

This paper is organized as follows. In Sec. II we introduce the model basics of RPV-SUSY and the lightest neutralino. In Sec. III, we introduce the detector setups of ANUBIS and MAPP, and explain the simulation procedure and signal estimation. The numerical results for two benchmark scenarios are presented in Sec. IV. In Sec. V we summarize our findings and provide an outlook.

II. MODEL BASICS OF RPV-SUSY, THE PRODUCTION AND DECAY OF THE $\tilde{\chi}_1^0$

Here, we introduce the RPV-SUSY model, and discuss the production and decay of the lightest neutralinos via RPV couplings. In RPV-SUSY, the MSSM superpotential is extended by the following renormalizable terms:

$$W_{\rm RPV} = \kappa_i L_i H_u + \frac{1}{2}\lambda_{ijk} L_i L_j E_k^c + \lambda'_{ijk} L_i Q_j D_k^c + \frac{1}{2}\lambda''_{ijk} U_i^c D_j^c D_k^c \,. \quad (1)$$

Here we use the notation as in Ref. [49]. In particular the λ, λ', λ'' are dimensionless Yukawa couplings, and $i, j, k \in \{1, 2, 3\}$ are generation indices. The first three sets of terms violate lepton number and the last violates baryon number. In order to avoid rapid proton decay we consider an additional baryon triality, B_3, symmetry imposed [50, 51], which allows only the lepton-number violating operators and is discrete gauge anomaly-free. For this work, we choose to consider only the $LQ\bar{D}$ operators. The lightest supersymmetric particle (LSP) is then no longer stable and decays into SM particles. In this study, we assume that the lightest neutralino is the LSP, which it need not be [52, 53].

Following Refs. [30, 39], we investigate 2 benchmark scenarios, where the $\tilde{\chi}_1^0$ LSP's are singly produced from either a charm or a bottom meson's rare decay, and then decay to a lighter meson with a displaced vertex to be reconstructed inside a detector. Such light GeV-scale, or lighter, neutralinos are necessarily binolike to avoid existing bounds [12, 13]. We perform the computation of the decay widths of the heavy mesons into the lightest neutralino and of the neutralinos into a lighter meson plus a neutral or charged lepton, with the analytic formulas given in Refs. [5, 13, 25, 30]. In each of these benchmark scenarios, two RPV couplings are assumed to be nonzero, responsible for the production and decay of $\tilde{\chi}_1^0$, respectively. We work directly at the low-energy scale, disregarding the possibility of multiple RPV couplings generated as a result of the renormalization group equations [54].

The RPV couplings are in general constrained by various experimentally measured observables. Such bounds usually depend on the relevant scalar fermion particles. See Refs. [23, 55–59] for reviews. Below we summarize the current bounds on both the single RPV couplings and coupling products that are relevant to the benchmark scenarios we study, extracted from Refs. [55, 58–60].

The current single couplings bounds are [58, 60]:

$$\lambda'_{112} < 0.030 + 0.16\,\frac{m_{\tilde{d}_R}}{1\ \rm TeV}\,, \quad (2)$$

$$\lambda'_{122} < 2\,\frac{m_{\tilde{s}_R}}{1\ \rm TeV}\,, \quad (3)$$

$$\lambda'_{131} < 0.19\,\frac{m_{\tilde{t}_L}}{1\ \rm TeV}\,, \quad (4)$$

and coupling products bounds are [55, 59]:

$$\sqrt{\lambda'_{122}\lambda'_{112}} < 4.7\times10^{-2}\,\frac{m_{\tilde{s}_R}}{1\ \rm TeV}\,, \quad (5)$$

$$\sqrt{\lambda'_{131}\lambda'_{112}} < 3.0\times10^{-3}\,\frac{m_{\tilde{e}_L}}{1\ \rm TeV}\,. \quad (6)$$

These bounds on the RPV couplings stem from different phenomenological origins, including meson decays and oscillations, atomic parity violation, as well as LHC Drell-Yan data and electroweak precision measurements from LEP and SLC. Consequently they depend on the masses of different sfermions. In this work, we assume

for simplicity degenerate sfermion masses, and will compare the sensitivity of ANUBIS and MAPP in the parameter space of the RPV-SUSY with the current experimental bounds. All the above bounds derive from R-parity conserving reactions, involving two insertions of an R-parity violating operator and one supersymmetric scalar propagator. Thus in each case the amplitude is proportional to $\lambda'^2/\tilde{m}^2$. The meson decays we consider below violate R-parity, as the initial state is R-parity even and the final state with one neutralino is R-parity odd. Thus the amplitudes are proportional to $\lambda'/\tilde{m}^2$, manifesting a different scaling behaviour.

Before we move to the next section, we briefly summarize the current lower bounds on sfermion masses derived from direct SUSY searches at the LHC, for the $LQ\bar{D}$ couplings considered in this work [53]. We find that while there is presently no relevant constraint on sneutrino, selectron, and sbottom masses, lower limits on the masses of first- and second-generation squarks and stops exist for λ'_{112} and λ'_{122} (though not for λ'_{131}). Assuming $m_{\tilde{\chi}_1^0} = 0.5\, m_{\tilde{q}}$ or $m_{\tilde{\chi}_1^0} = 0.9\, m_{\tilde{q}}$, the bounds on squark masses for λ'_{112} and λ'_{122} are 1160 and 1315 GeV, respectively [61]. Further, the present bounds on $m_{\tilde{t}}$ are 890 GeV for λ'_{1bc} with $b, c \in \{1, 2\}$, assuming $m_{\chi_1^\pm} = 100$ GeV [62]. Since these bounds are in general around 1 TeV, we will focus on two benchmark values of the degenerate sfermion masses, 1 TeV and 5 TeV, when we compare the sensitivity reach of ANUBIS and MAPP to the existing limits in Sec. IV.

III. EXPERIMENTAL SETUPS AND SIMULATION PROCEDURE

In this section we introduce the detector setups of the proposed experiments ANUBIS and MAPP, explain the simulation procedure, and discuss the estimate of signal-event numbers.

At both experiments, there are various potential background sources such as long-lived SM hadrons decays and cosmic rays. Such background events can be effectively reduced to the negligible level by *e.g.* charged-particle vetos and directional cuts, as discussed in Refs. [45, 47]. Accordingly we assume 0 background events for the sensitivity study in this paper. Furthermore, since the detailed detector information of these two experiments are not yet available, for simplicity we assume 100% detector efficiencies here.

A. ANUBIS and MAPP

ANUBIS is proposed as a cylindrical detector making use of one of the installation shafts at the ATLAS or CMS IP. Sketches of the experiment, reproduced from Ref. [46], are presented in Fig. 1 from two perspectives, where a sample LLP with polar angle θ_i is labeled with a dashed arrow. ANUBIS has a height, l_v, of 56 m and a diameter l_h of 18 m, so that the fiducial region consists of approximately $\sim 14{,}250\,\mathrm{m}^3$. It has a horizontal (vertical) distance d_h (d_v) of 5 (24) m from the IP. Four tracking stations are planned to be installed in parallel, with intervals of 18.5 m.

Compared to the other proposed dedicated far-detector experiments at the LHC, ANUBIS has several advantages. First, with its location inside one of the service shafts above the ATLAS/CMS IP, it can be particularly sensitive to LLPs traveling at a larger polar angle. It can be integrated directly with the ATLAS/CMS experiment, extending the sensitivity of these currently running experiments. A total integrated luminosity as large as 3 ab^{-1} at the HL-LHC is expected for the ANUBIS experiment.

MAPP is located in the UGCI gallery at the IP8 at the LHC, close to the MoEDAL detector ("Monopole and Exotics Detector At the LHC"). The first phase of the experiment known as MAPP1 is planned to be in operation during the LHC RUN-3 with an integrated luminosity of 30 fb^{-1}. MAPP1 consists of two sub-detectors: MAPP-mCP to detect minimally charged particles and MAPP-LLP to search for neutral LLPs. We consider the latter with an approximate fiducial volume of ~ 130 m^3.

The detector can be placed at multiple positions in the UGCI gallery with an angular range of 5° to 25°. Depending on the angle, the detector is shielded by 25 to 55 m of rock. We consider the position at 5° with a distance of 55 m. Additionally, the detector is shielded by 100 m of rock above it, so that we assume no background for the MAPP experiment.

After RUN-3 an upgrade of the detector known as MAPP2 is planned, in which the fiducial region is extended to cover almost the whole gallery with a volume of ~ 430 m^3. The sketches of both detectors are given in Fig. 2, where the MAPP1 detector is shown in green only while MAPP2 will occupy both the green and red regions. Similar to Fig. 1, a sample event with polar angle θ_i is illustrated in the figures.

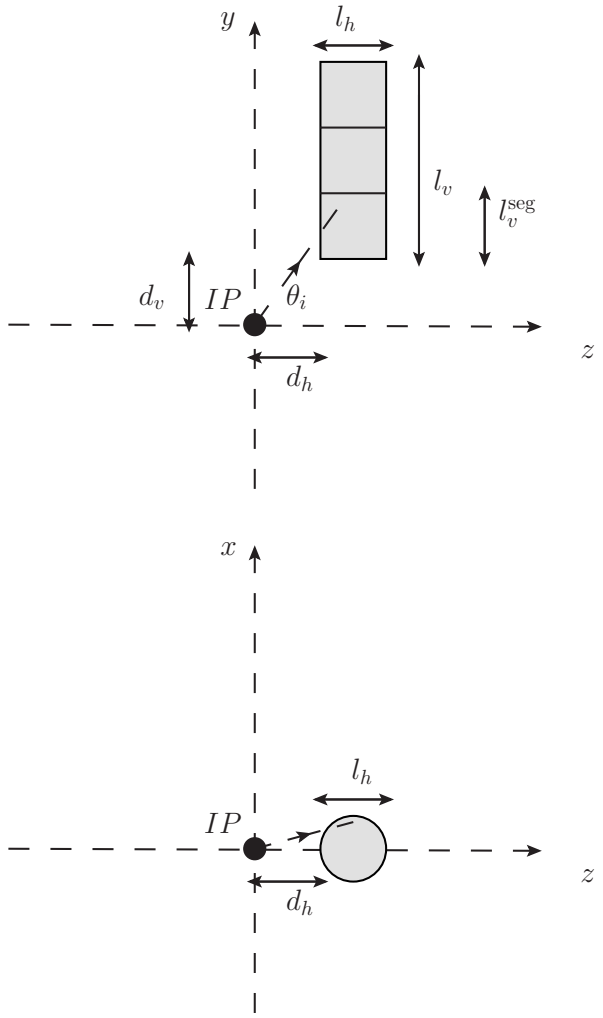


FIG. 1. The profile sketches of the ANUBIS detector in the $y-z$ (looking from the side) and the $x-z$ (looking from the top down) planes, respectively, extracted from Ref. [46]. A sample LLP-event with polar angle θ_i is included in the sketches.

B. Simulation and Signal Event Estimate

We proceed to describe the simulation procedure and the estimate of the number of signal events in each of these experiments.

Since we consider only the production of the lightest neutralinos from rare decays of charm and bottom mesons, we can express the total number of produced $\tilde{\chi}_1^0$'s in terms of the total number of produced mesons N_M, their lifetime τ_M, and the meson partial decay width into $\tilde{\chi}_1^0$ and a lepton:

$$N_{\tilde{\chi}_1^0}^{\text{prod}} = \sum_M N_M \cdot \Gamma(M \to \tilde{\chi}_1^0 + l_i/\nu_i) \cdot \tau_M, \qquad (7)$$

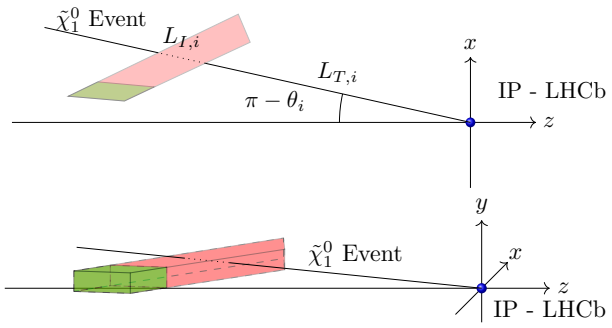


FIG. 2. Sketches of `MAPP1` (green) and `MAPP2` (red+green) in the x-z plane, *i.e.* viewed from above, and in three dimensions, with the y-axis pointing vertically upwards. A sample event is shown hitting `MAPP2` but not `MAPP1`.

Meson M	$D_s^{\pm}$	$B^0/\bar{B}^0$
N_M	6.62×10^{15}	1.46×10^{15}

TABLE I. The total number of D- and B-mesons expected at `ANUBIS` for an integrated luminosity of 3 ab^{-1} over the full solid angle 4π. For `MAPP1` and `MAPP2` we scale the results to the respective integrated luminosities, 30 fb^{-1} and 300 fb^{-1}.

where $i = 1, 2, 3$ is the lepton generation.

In principle one can consider the lightest neutralinos produced from either a pseudoscalar or a vector meson decay. However, the lifetime of the vector mesons is usually several orders of magnitude (up to 9 orders of magnitude for D-mesons for instance) lower than that of their pseudoscalar counterparts. In order to produce sufficiently many neutralinos from such vector meson decays mediated by an RPV coupling, the coupling has to be much larger than the current upper experimental bounds. Thus, we only consider pseudoscalar mesons for the neutralino production. Considering both D- and B-mesons rare decays, we are able to explore $\tilde{\chi}_1^0$ masses up to several GeV and down to a few hundred MeV. We follow the procedure given in Ref. [39] to extract the total number of the charm and bottom mesons that are relevant to this study, respectively. This is based on the experimental results of charm meson and $b-$quark production cross sections published by the LHCb collaboration [63, 64], and the kinematic extrapolation to the complete solid-angle coverage with the numerical tool `FONLL` [65–68], and B-meson fragmentation by using `Pythia 8` [69, 70]. We summarize the results in Table I.[2]

[2] The numbers are slightly different from those given in Ref. [39]. We have corrected some minor errors in that paper.

The lightest neutralinos may undergo two-body decays into either charged or neutral final states. While both types contribute to the total decay width of $\tilde{\chi}_1^0$, only the charged final states can be easily used for the displaced-vertex reconstruction. We therefore consider only these as visible. The number of observed lightest neutralino decays can be expressed as

$$N_{\tilde{\chi}_1^0}^{\text{obs}} = N_{\tilde{\chi}_1^0}^{\text{prod}} \cdot \left\langle P\left[\tilde{\chi}_1^0 \text{ in d.r.}\right]\right\rangle \cdot \text{BR}\left(\tilde{\chi}_1^0 \to \text{char.}\right), \quad (8)$$

where $\left\langle P\left[\tilde{\chi}_1^0 \text{ in d.r.}\right]\right\rangle$ denotes the average probability of the $\tilde{\chi}_1^0$ to decay inside the detectable region (d.r.) of a given detector and "char." labels charged final states. We perform a Monte-Carlo (MC) simulation with `Pythia 8` in order to determine $\left\langle P\left[\tilde{\chi}_1^0 \text{ in d.r.}\right]\right\rangle$. We simulate $N_{\tilde{\chi}_1^0}^{\text{MC}}$ MC-events and calculate $\left\langle P\left[\tilde{\chi}_1^0 \text{ in d.r.}\right]\right\rangle$ with the following formula:

$$\left\langle P\left[\tilde{\chi}_1^0 \text{ in d.r.}\right]\right\rangle = \frac{1}{N_{\tilde{\chi}_1^0}^{MC}} \sum_{i=1}^{N_{\tilde{\chi}_1^0}^{MC}} P\left[\left(\tilde{\chi}_1^0\right)_i \text{ in d.r.}\right], \quad (9)$$

where $P\left[\left(\tilde{\chi}_1^0\right)_i \text{ in d.r.}\right]$ is the probability of an individual simulated $\tilde{\chi}_1^0$ to decay in the d.r. The calculation of the individual decay probability takes into account the geometries of the respective detector and the kinematics of an individual $\tilde{\chi}_1^0$, and is explained in more detail below.

To perform the MC simulation, we use two modules, `HardQCD:hardccbar` and `HardQCD:hardbbbar` implemented in `Pythia 8`, in order to simulate D- and B-meson production in $pp-$collisions with the center-of-mass energy $\sqrt{s} = 14$ TeV. For each parameter point, we simulate 2×10^6 collisions for the bottom and 2×10^7 collisions for the charm scenarios. We force the meson relevant for each benchmark scenario to exclusively decay into the lightest neutralino plus the accompanying lepton, in order to achieve the maximal number of statistics for estimating the average decay probability. We then compute the number of expected neutralino decays by including the total number of the mother meson produced and its decay branching ratio into $\tilde{\chi}_1^0$.

The calculation of the individual decay probabilities in the detector requires the kinematic information of each simulated neutralino. With the mass $m_{\tilde{\chi}_1^0}$ and the 4-momentum information (E_i, θ_i, ϕ_i) of the i-th simulated neutralino provided by `Pythia 8`, we can calculate the relativistic quantities with the following expressions:

$$\gamma_i = E_i/m_{\tilde{\chi}_1^0}, \quad (10)$$

$$\beta_i = \sqrt{\gamma_i^2 - 1}/\gamma_i, \quad (11)$$

$$\lambda_i = \beta_i\gamma_i/\Gamma_{\text{tot}}(\tilde{\chi}_1^0), \quad (12)$$

$$\beta_i^z = p_i^z/E_i, \quad (13)$$

$$\lambda_i^z = \beta_i^z\gamma_i/\Gamma_{\text{tot}}(\tilde{\chi}_1^0), \quad (14)$$

where γ_i is the Lorentz boost factor of the neutralino, β_i (β_i^z) the relativistic speed (the velocity in the collider-beam direction), $\Gamma_{\text{tot}}(\tilde{\chi}_1^0)$ the total decay width of the neutralino, λ_i (λ_i^z) the boosted decay length in the traveling direction (in the beam direction).

C. The Individual Decay Probability

The traveling direction of an LLP is defined by the polar and azimuthal angles. $P\left[\left(\tilde{\chi}_1^0\right)_i \text{ in d.r.}\right]$ can then be estimated by

$$P\left[\left(\tilde{\chi}_1^0\right)_i \text{ in d.r.}\right] = e^{-\frac{L_{T,i}}{\lambda_i}}\left(1 - e^{-\frac{L_{I,i}}{\lambda_i}}\right), \quad (15)$$

in the case that the lightest neutralino travels inside the solid angle protruded by the detector. Otherwise the decay probability in the detector is 0. $L_{T,i}$ is the distance from the IP to the closest point of the detector, while $L_{I,i}$ is the distance the i-th simulated neutralino would travel inside the detector given its traveling direction, if it does not decay before it leaves the detector. Both $L_{T,i} = L_{T,i}(\theta_i, \phi_i)$ and $L_{I,i} = L_{I,i}(\theta_i, \phi_i)$ are functions of the angles θ_i, ϕ_i as well as the geometry of the detector at hand.

1. *ANUBIS*

In order to estimate the individual decay probability of an LLP inside the `ANUBIS` detector, we follow the same procedure as in Ref. [46]. `ANUBIS` has 4 equally spaced tracking stations, between which we divide the detectable region into 3 segments of height $l_v^{\text{seg}} = 18.67$ m. For each of these regions we calculate separately $P_j\left[\left(\tilde{\chi}_1^0\right)_i \text{ in d.r.}\right]$ with $j = 1, 2, 3$ and then sum over all three probabilities. If one of the two following conditions is met

$$\tan\theta_i \leq \frac{d_v + (j-1)\cdot l_v^{\text{seg}}}{d_h + l_h}, \quad (16)$$

$$\tan\theta_i \geq \frac{d_v + j\cdot l_v^{\text{seg}}}{d_h}, \quad (17)$$

P_j is 0. In the first case the neutralino flies below segment j, thus missing it. In the second case it flies above segment j. Otherwise we have

$$P\left[\left(\tilde{\chi}_1^0\right)_i \text{ in d.r.}\right] = \sum_{j=1}^{3} \frac{\delta\phi^j}{2\pi} \cdot e^{-\frac{L^j_{T,i}}{\lambda^z_i}} \cdot \left(1 - e^{-\frac{L^j_{I,i}}{\lambda^z_i}}\right), \tag{18}$$

where

$$\delta\phi^j = 2\arctan\frac{l_h/2}{d_v + (2j-1)/2 \cdot l_v^{\text{seg}}}, \tag{19}$$

$$L^j_{T,i} = \min\left[\max\left(d_h, \frac{d_v + (j-1)\cdot l_v^{\text{seg}}}{\tan\theta_i}\right), d_h + l_h\right], \tag{20}$$

$$L^j_{I,i} = \min\left[\max\left(d_h, \frac{d_v + j\cdot l_v^{\text{seg}}}{\tan\theta_i}\right), d_h + l_h\right] - L^j_i\,. \tag{21}$$

We do not determine the probability exactly for the azimuthal coverage. We assume the events are isotropic in ϕ and consider for each detector segment a cone around the y-axis to half the segment height. For the first segment we then have that $(\phi_i - \pi/2) \in [-\delta\phi, +\delta\phi]$, where $\tan\delta\phi/2 = (l_h/2)/(d_v + l_v^{\text{seg}}/2)$. Correspondingly for the other segments as in Eq. (19). The azimuthal coverage is then accounted for with the prefactor $\delta\phi^j/2\pi$ in Eq. (18). Using this approximation for the location of the ANUBIS detector, and the probability for it to be hit by a particle flying from the IP, we find a geometric coverage of the total solid angle of about 1.34%.[3]

2. MAPP

Because of the less regular orientation of the MAPP detectors, it is not straightforward to compute the individual decay probability, as for ANUBIS. Instead, we simulate the MAPP detectors in an exact way in three-dimensional space. For this we construct a virtual model of the detectors based on their corner points. This defines the surfaces of the detectors and thus the entire volume. Using the information of the polar and azimuthal angles of each simulated neutralino, our program determines whether the neutralino is traveling in a direction inside the detector window, and if so computes the $L_{T,i}$ and $L_{I,i}$ as given in Eq. (15), with which the individual decay probability in the MAPP detectors can be exactly determined. Using this more precise method, we find that MAPP1 and MAPP2 geometrically cover about 0.17% and 0.68% of the total solid angle, respectively.

We note that in principle this method can also be used for a cylindrical detector such as ANUBIS. However, given the rather small azimuthal-angle coverage of the ANUBIS detector, the amount of simulation increases drastically in order to reduce the numerical uncertainty to a sufficiently small level. Therefore, we use Eq. (18), which does not require a too large number of simulated events and at the same time is a sufficiently good approximation. With this exact geometry of the ANUBIS detector, the solid-angle coverage is estimated to be 1.79%, which is slightly larger than that obtained by the approximate geometry (see Eq. (18)). Thus our previous estimate is conservative. The effect on the sensitivity in each RPV coupling enters via the square root, thus the effect is about 15% in each coupling.

IV. NUMERICAL RESULTS FOR THE BENCHMARK SCENARIOS

Here we present our numerical results. In Refs. [30, 39] a variety of benchmark scenarios involving different $LQ\bar{D}$ couplings were investigated. These scenarios consider the production of light neutralinos via the rare decay of charged or neutral charm and bottom mesons. The neutralinos subsequently decay into lighter mesons. In each scenario, two $LQ\bar{D}$ couplings are switched on, one responsible for the production and one for the decay of the neutralinos. In this work, we focus on only two specific benchmark scenarios, one for charmed and one for bottom mesons.

The relevant matrix elements for the production and decay of the neutralinos are given in Ref. [30]. The effective production and decay operators are proportional to the RPV-couplings scaled to the squared sfermion mass $\lambda'/m^2_{\tilde{f}}$. This is in contrast to the existing low-energy bounds listed in Eqs. (2)-(6), which scale with the sfermion masses as $\lambda'^2/m^2_{\tilde{f}}$ or $\lambda'/m_{\tilde{f}}$, for reasons explained in Sec II. For simplicity, we assume degenerate sfermion masses, so that we are left with three free parameters for each benchmark scenario: the scaled production and decay couplings $\lambda'_{P,ijk}/m^2_{\tilde{f}}$ and $\lambda'_{D,i'j'k'}/m^2_{\tilde{f}}$, and the neutralino mass $m_{\tilde{\chi}_1^0}$. With three independent parameters, we choose to present the sensitivities in two types of parameter planes. First, we set the two λ'-couplings to be equal and lay out the dependence

[3] The solid angle coverage is determined using Monte-Carlo integration with 10^6 events. We display the mean solid angle, $\bar{\Omega}$, of 100 such integrations. The relative standard deviation ($\sigma/\bar{\Omega}$) is $< 0.3\%$ for all mentioned solid angles.

λ'_P for production	λ'_{122}
λ'_D for decay	λ'_{112}
produced meson(s)	D_s
visible final state(s)	$K^{\pm}+e^{\mp}$, $K^{*\pm}+e^{\mp}$
invisible final state(s) via λ'_P	$(\eta,\eta',\phi)+(\nu_e,\overline{\nu}_e)$
invisible final state(s) via λ'_D	$\left(K_L^0,K_S^0,K^*\right)+(\nu_e,\overline{\nu}_e)$

TABLE II. Features of the charmed benchmark scenario.

on the neutralino mass: $\lambda'_{P,ijk}/m^2_{\tilde{f}} = \lambda'_{D,i'j'k'}/m^2_{\tilde{f}}$ vs. $m_{\tilde{\chi}_1^0}$. The other parameter plane chosen is $\lambda'_{P,ijk}/m^2_{\tilde{f}}$ vs. $\lambda'_{D,i'j'k'}/m^2_{\tilde{f}}$ for three fixed neutralino masses, where we vary the two $LQ\bar{D}-$couplings independently.

We further display the sensitivities in the plane Br vs. $c\tau$, where Br denotes the decay branching ratio of the mother meson times that of the neutralino into charged products, and $c\tau$ is the proper decay length of the neutralino. If the decay topologies are similar, these results should not be different qualitatively in the context of other theoretical models. As mentioned, we consider only the charged final states can be detected and used for the DV reconstruction.

A. Benchmark scenario 1 - charmed Meson D_s

For the first scenario we consider λ'_{122} and λ'_{112} to be non-zero, mediating the production and decay of the lightest neutralino, respectively. We start with a D_s-meson decaying promptly via the $L_1Q_2\bar{D}_2$ operator:

$$D_s \to \tilde{\chi}_1^0 + e^{\pm}. \tag{22}$$

Afterwards the neutralino travels a macroscopic distance before decaying with a displaced vertex via λ'_{112} into either charged or neutral states:

$$\tilde{\chi}_1^0 \to \begin{cases} K^{(*)\pm}+e^{\mp}\,, \\ K^0_{L/S}/K^{*0}+\nu_e\,. \end{cases} \tag{23}$$

In addition the production coupling induces invisible neutralino decays:

$$\tilde{\chi}_1^0 \to \begin{cases} \eta/\eta'+\nu_e\,, \\ \phi+\nu_e\,, \end{cases} \tag{24}$$

which must be taken into account when computing the total decay width. The relevant features of benchmark scenario 1 are summarized in Table II.

In Fig. 3 we present the model-dependent results for this benchmark scenario. The left column contains plots in the plane $\lambda'/m^2_{\tilde{f}}$ vs. $m_{\tilde{\chi}_0^1}$ for ANUBIS, MAPP1, and MAPP2 experiments, respectively, where we impose $\lambda'_{122}=\lambda'_{112}$. In these plots we show contours of three different numbers of signal events with the light, medium, and dark blue areas corresponding to parameter regions with >3, $>3\times10^3$, and $>3\times10^6$ signal events, respectively. Furthermore, the 3-event isocurve is extended by the dashed line which gives the sensitivity reach if the neutral final states, the lower set of decays in Eq. (23) and the decays in Eq. (24), can be detected. Current bounds on the RPV-couplings as given in Eq. (2) (Eq. (5)) are shown with solid (dot-dashed) horizontal lines. For the single coupling bounds on λ'_P and λ'_D, we show only the stronger one for sfermion masses of 1 TeV and 5 TeV, while for the bound on the product of the two RPV couplings ($\sqrt{\lambda'_{122}\lambda'_{112}}/m^2_{\tilde{f}}$) we consider only one sfermion mass at 1 TeV.

The sensitive neutralino mass range for these experiments are all similar and constrained mainly by the kinematics of the scenario:

$$(M_{K^\pm}+m_e) < m_{\tilde{\chi}_1^0} < (M_{D_s}-m_e)\,. \tag{25}$$

Beyond this, the sensitivities are dependent only to a small extent on the neutralino mass, depicted here by the slope of the lower edge of the various sensitivity regions in the plots in the left column. The sensitivity regions are bounded from above, as for large couplings the neutralinos would decay too fast to reach the detector. They are bounded from below since for small couplings there is both insufficient production of the neutralinos and a too large decay length. The slope of the upper edge of the sensitivity regions can be understood as follows. Increasing the two RPV couplings and decreasing the neutralino mass simultaneously, the observed number of signal events increase in general. This is because a large λ'_P leads to enhancement in the neutralino production, while the increase in λ'_D and decrease in $m_{\tilde{\chi}_1^0}$ retains the decay width and the average decay probabilities in the detector.

In benchmark scenario 1, all three experiments may probe parameter regions beyond the current RPV-coupling bounds, to different extents. While the sensitivity of MAPP1 beyond the current limits would be less than a factor 2 in $\lambda'/m^2_{\tilde{f}}$, its upgraded version, MAPP2, may extend the reach of MAPP1 by a further factor of ~ 3, by virtue of its larger volume and the increased integrated luminosity. Among the three experiments studied in this work, ANUBIS shows the best sensitivity reach, exceeding the current limits by a factor ~ 8 in $\lambda'/m^2_{\tilde{f}}$. This can be attributed to its even greater integrated luminosity and a larger solid-angle coverage.

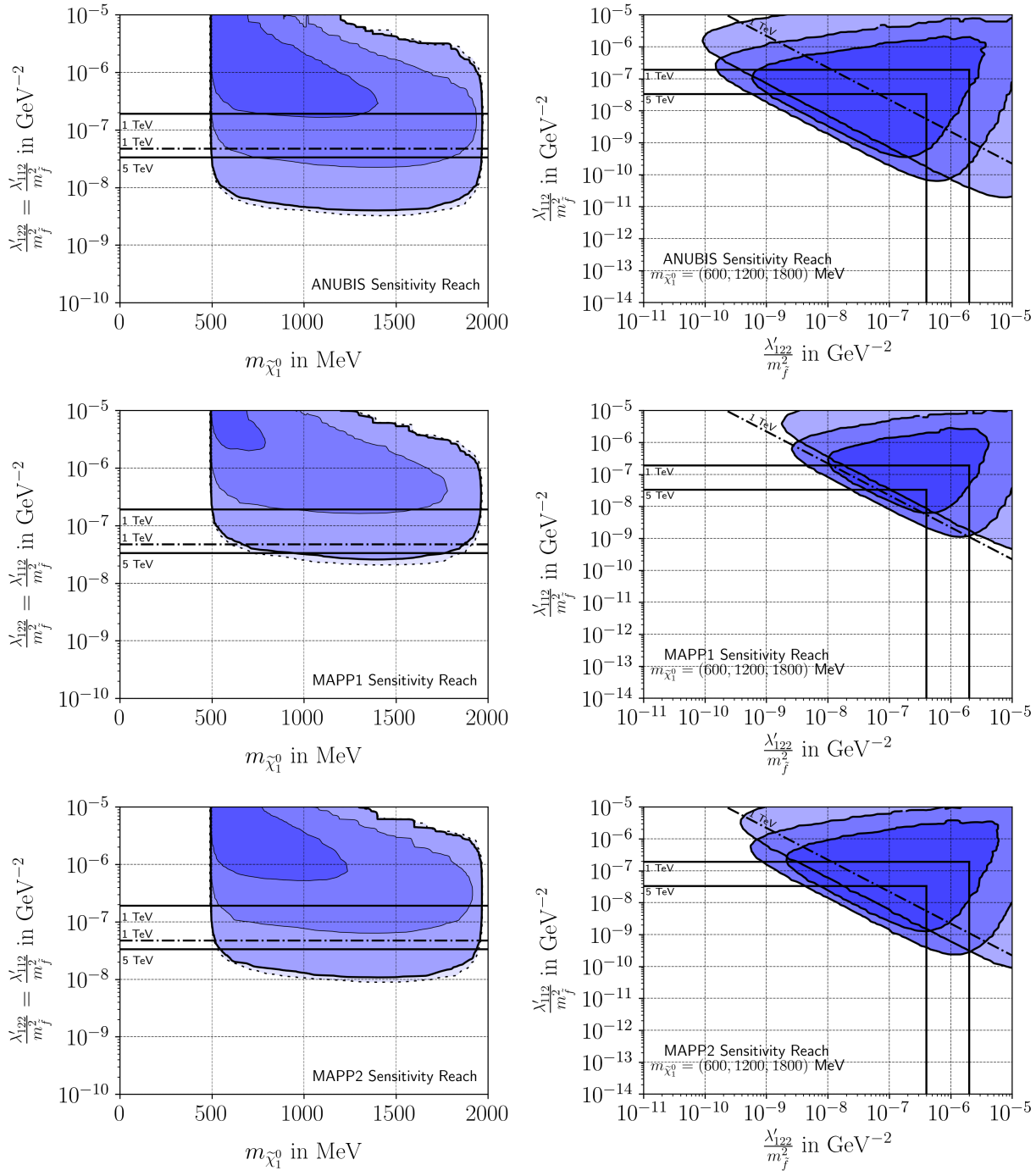


FIG. 3. Estimated sensitivity reach for `ANUBIS`, `MAPP1`, and `MAPP2` for benchmark scenario 1, with charmed mesons. For the left column we demand the two $LQ\bar{D}$ couplings to be equal and detail the reach as a function of the neutralino mass. The isocurves represent 3 events (light blue), 3×10^3 events (medium blue), and 3×10^6 (dark blue). The dashed isocurve is an extension of the 3-event isocurves, if the neutral 'invisible' decays can be observed in the detector. We implement the stronger current coupling bound (here for λ'_{112}) for two different sfermion masses, $m_{\tilde{f}} = 1\,\text{TeV}$ and $5\,\text{TeV}$ (solid), and the product bound for $m_{\tilde{f}} = 1\,\text{TeV}$ (dot-dashed). Depicted in the right column are 3-event isocurves on the λ'_D vs. λ'_P parameter region for 3 specific neutralino masses, namely 600 MeV (light blue), 1200 MeV (medium blue), and 1800 MeV (dark blue). Current upper limits on the individual couplings for two sfermions masses $m_{\tilde{f}} = 1\,\text{TeV}$ and $5\,\text{TeV}$ (solid), as well as the product limit for the sfermion mass $m_{\tilde{f}} = 1$ TeV (dot-dashed) are presented.

The plots in the right column of Fig. 3 are shown in the plane $\lambda'_D/m^2_{\tilde{f}}$ vs. $\lambda'_P/m^2_{\tilde{f}}$. 3-event isocurves in different colors are presented for three fixed neutralino masses: 600 (light blue), 1200 (medium blue), and 1800 MeV (dark blue). These choices of the neutralino mass correspond approximately to the lower and higher ends, and the middle point of the mass range allowed by the kinematics, as discussed above. As in the plots on the left, we included present experimental bounds on both single couplings and the couplings' product for different sfermion masses.

The isocurves are bounded from all four sides. With a too large/small λ'_D (y-axis), the lightest neutralinos decays too early/late, leading to a too small average decay probability in the detectors. When λ'_P (x-axis) is too small, there is insufficient production of the neutralinos. With a too large λ'_P, the lightest neutralinos would also decay before they reach the detector. This is specific for this scenario, as λ'_P also induces invisible decays of the neutralino and hence enhances its total decay width.

We find that ANUBIS, MAPP1, and MAPP2 can all be sensitive to new parameter regions beyond the current RPV limits for sfermion masses of the order of 1 TeV. As observed in the plots in the left column, compared to MAPP1, MAPP2 shows better sensitivity reach while ANUBIS is expected to have the strongest performance. Assuming $m_{\tilde{f}} = 5\,\text{TeV}$ as a reference value, MAPP1 improves the current bounds on λ'_{122} and λ'_{112} by approximately one order of magnitude, whereas MAPP2 and ANUBIS improve them by more than two orders of magnitude. In general among the three masses considered, $m_{\tilde{\chi}^0_1} = 1200\,\text{MeV}$ probes the largest part of the parameter regions that are still allowed by the present limits.

In Fig. 4, we show the model-independent results for benchmark scenario 1 in the plane Br vs. $c\tau$ for two neutralino masses. Here we specify "Br" with the following expressions:

$$\text{Br} \equiv \text{Br}\left(D_s^{\pm} \to \tilde{\chi}^0_1 + e^{\pm}\right) \cdot \text{Br}\left(\tilde{\chi}^0_1 \to K^{(*)\pm} + e^{\mp}\right). \quad (26)$$

The solid pink curves denote MAPP1, the dashed red curves MAPP2, and the dot-dashed blue curves ANUBIS. The lighter mass 600 MeV correlates to the lighter color, while the darker color is for a mass of 1200 MeV. The relative comparison between these experiments is similar to that shown in Fig. 3. The minimum of each curve gives the lowest reach in Br, and its corresponding position in the proper lifetime. For this scenario, ANUBIS may reach $\text{Br} \approx 7 \times 10^{-13}$, while the two MAPP programs are less sensitive by more than one order of magnitude.

In order to understand the resulting lowest points in Br: $(c\tau)_{\text{min}}$, in Fig. 4, we first consider the distance from

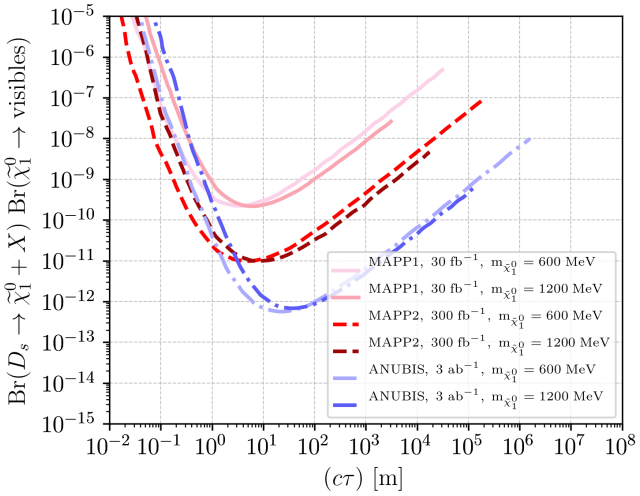


FIG. 4. Sensitivity estimates for a neutral long-lived fermion in a model-independent description for the charmed benchmark scenario 1 using our neutralino estimates. For each detector the estimates for two light neutralino masses are depicted. For benchmark scenario 1 these masses are 600 and 1200 MeV. The lighter colors are used for the lighter mass. MAPP1 is illustrated with a pink solid curve, MAPP2 red with a dashed line and ANUBIS blue with a dot-dashed line.

Scenario	$m_{\tilde{\chi}^0_1}$ [MeV]	$\langle\beta\gamma\rangle_{\texttt{ANUBIS}}$	$\langle\beta\gamma\rangle_{\texttt{MAPP1}}$	$\langle\beta\gamma\rangle_{\texttt{MAPP2}}$
1 - D_s	600	2.78	24.45	17.22
1 - D_s	1200	2.94	16.63	13.26
2 - $B^0/\overline{B}^0$	1000	5.56	37.86	26.77
2 - $B^0/\overline{B}^0$	3000	2.62	16.42	12.72

TABLE III. Average boost factors of the neutralinos for the three detectors and both benchmark scenarios.

the IP to the middle position of the detector, $\langle L\rangle$. For the three detectors we have

$$\langle L\rangle = \begin{cases} 53.85\ \text{m} & \text{for ANUBIS}, \\ 55.06\ \text{m} & \text{for MAPP1}, \\ 46.71\ \text{m} & \text{for MAPP2}. \end{cases} \quad (27)$$

We estimate the average boost $\langle\beta\gamma\rangle$ of the produced neutralinos for each detector with our numerical simulation, with the results listed in Table III. We note that for the two MAPP programs the relevant neutralinos have similar average boost factors while the neutralinos traveling inside the ANUBIS window have an average boost factor approximately one order of magnitude smaller. This is mainly due to the difference in the polar-angle coverage of these experiments. Since at the LHC the charm and bottom mesons that would decay to the light neutralinos are on average highly boosted in the forward direction, the neutralinos that travel at a larger polar angle tend to

λ'_P for production	λ'_{131}
λ'_D for decay	λ'_{112}
produced meson(s)	B^0, $\overline{B}^0$
visible final state(s)	$K^\pm + e^\mp$, $K^{*\pm} + e^\mp$
invisible final state(s) via λ'_P	None
invisible final state(s) via λ'_D	$\left(K^0_L, K^0_S, K^*\right) + (\nu_e, \overline{\nu}_e)$

TABLE IV. Features of the bottomed benchmark scenario.

be less energetic. As ANUBIS covers polar angles larger than MAPP1 and MAPP2, the neutralinos going into ANUBIS are expected to have a smaller boost factor.

The minima of the curves are found to correspond to

$$(c\tau)_{\min} \approx \langle L \rangle \,/\, \langle \beta\gamma \rangle \,. \tag{28}$$

This corresponds to the point of highest sensitivity to the product of branching ratios. Taking $m_{\tilde{\chi}^0_1} = 600\,\text{MeV}$ as an example, we obtain

$$(c\tau)_{\min} = \begin{cases} 19.37 \text{ m} & \text{for ANUBIS}, \\ 2.25 \text{ m} & \text{for MAPP1}, \\ 2.71 \text{ m} & \text{for MAPP2}, \end{cases} \tag{29}$$

in approximate agreement with the minima of the lighter-colored curves in Fig. 4. The value of $(\text{Br})^2$ at $(c\tau)_{\min}$ depends on the angular coverage of the detector and the integrated luminosity.

B. Benchmark scenario 2 - bottomed Meson $B^0, \overline{B}^0$

Next, we consider neutral bottom mesons B^0 decaying to a neutralino plus a neutrino via the coupling λ'_{131}. The decay of the lightest neutralino into a kaon proceeds via the same coupling λ'_{112} as that considered in the previous benchmark scenario. The characterizing features of this benchmark are summarized in Table IV. This extends the mass range for the neutralino considerably because of the larger mass of the B-meson:

$$(M_{K^\pm} + m_e) < m_{\tilde{\chi}^0_1} < (M_{B^0} - m_{\nu_e}) \,. \tag{30}$$

We present the exclusion limits in the $\lambda'_P/m^2_{\tilde{f}} = \lambda'_D/m^2_{\tilde{f}}$ vs. $m_{\tilde{\chi}^0_1}$ as well as the $\lambda'_D/m^2_{\tilde{f}}$ vs. $\lambda'_P/m^2_{\tilde{f}}$ plane in Fig. 5. As in the previous scenario for the latter plane we consider three neutralino masses, which are 1000 MeV, 3000 MeV, and 5000 MeV here. In the $\lambda'_P/m^2_{\tilde{f}} = \lambda'_D/m^2_{\tilde{f}}$ vs. $m_{\tilde{\chi}^0_1}$ plane we observe a similar pattern as before. The sensitivity reach is mostly independent of the neutralino mass, except for the region close to the meson masses. The reach is bounded from above as the neutralino would decay too fast and below, where the neutralino production and the decay would be insufficient. We can extend the sensitivity reach slightly, if we were able to detect neutral final states.

MAPP2 enhances the sensitivity reach of MAPP1 due to the increased volume and integrated luminosity. However, both forms of the MAPP detector are only sensitive beyond the current single coupling limits by factors between 5 and 10, but not beyond the coupling product limit of this scenario for a sfermion mass of $m_{\tilde{f}} = 1\,\text{TeV}$. This lack of sensitivity of the MAPP detectors to reach the current coupling product limit, which depends on the selectron mass only, can potentially be reduced to some extent, if non-degenerate sfermion masses are assumed and the lightest allowed values of sfermions masses are taken. Even in that limit, we do not expect the MAPP programs to exceed the coupling product limit by much. ANUBIS has the greatest reach out of all 3 detectors, which extends beyond the coupling limits. Next, we consider the $\lambda'_D/m^2_{\tilde{f}}$ vs. $\lambda'_P/m^2_{\tilde{f}}$ plane. An important difference compared to the first scenario is that now the production coupling does not lead to neutralino decay modes and consequently we are not bounded from the right side for large values of λ'_P in Fig. 5. Comparing with the current bounds on the RPV couplings, ANUBIS may explore parameter regions that are still allowed, while the sensitive regions of MAPP1 and MAPP2 are almost completely ruled out by the current limit on the product of the two RPV couplings for $m_{\tilde{f}} = 1\,\text{TeV}$. For the medium neutralino mass at 3000 MeV, ANUBIS may probe $\lambda'_{131}/m^2_{\tilde{f}}$ ($\lambda'_{112}/m^2_{\tilde{f}}$) down to 7×10^{-11} GeV^{-2} (4×10^{-11} GeV^{-2}) at the upper limit of $\lambda'_{112}/m^2_{\tilde{f}}$ ($\lambda'_{131}/m^2_{\tilde{f}}$) for $m^2_{\tilde{f}} = 5$ TeV.

Lastly, we consider the representation for topologically identical theoretical models in Fig. 6 for $m_{\tilde{\chi}^0_1} = 1000$ MeV and 3000 MeV. The MAPP1 and MAPP2 lowest reach differs by more than one order of magnitude, while the ANUBIS reach in $\text{Br} \simeq 2 \times 10^{-12}$ is even stronger again by more than another order of magnitude. Considering the average lengths to the detector $\langle L \rangle$ from Eq. (27) and average boosts $\langle \beta\gamma \rangle$ from Tab. III for a neutralino mass $m_{\tilde{\chi}^0_1} = 1$ GeV, the position of the lowest reach should be

$$(c\tau)_{\min} = \begin{cases} 9.69 \text{ m} & \text{for ANUBIS}, \\ 1.45 \text{ m} & \text{for MAPP1}, \\ 1.74 \text{ m} & \text{for MAPP2}. \end{cases} \tag{31}$$

This approximately coincides with the valley positions in Fig. 6.

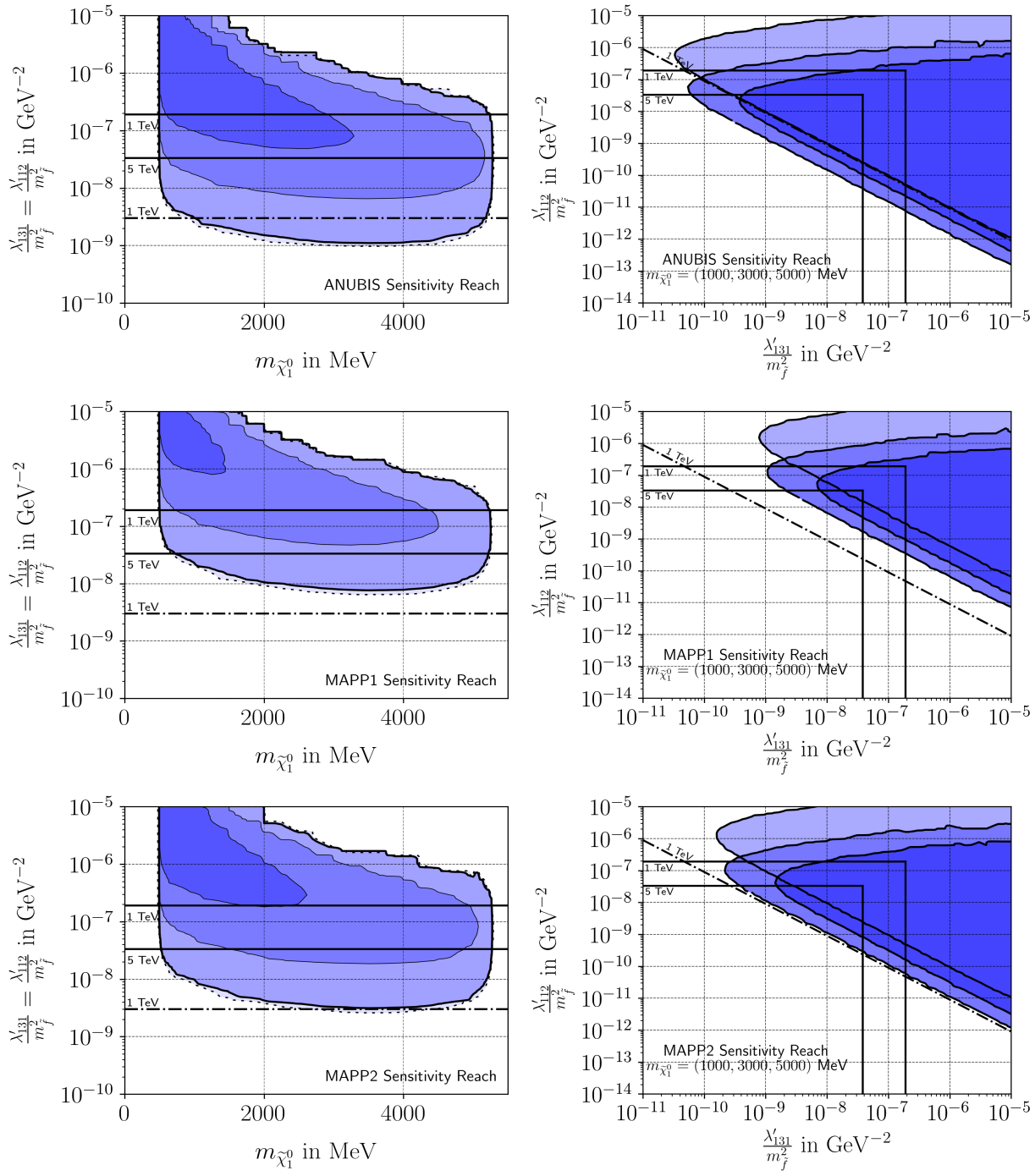


FIG. 5. Estimated sensitivity reach for `ANUBIS`, `MAPP1`, and `MAPP2` in the $\lambda'_{131}/m^2_{\tilde{f}}$ vs. $\lambda'_{112}/m^2_{\tilde{f}}$ parameter plane for the bottomed benchmark scenario. The labeling is similar to that in Fig. 3, whereas in the right column the neutralino masses considered now are $m_{\tilde{\chi}^0_1} = 1000$ MeV, 3000 MeV, and 5000 MeV colored as light blue, medium blue, and dark blue, respectively.

C. Comparison to previously considered Detectors

In previous works several detectors were studied for the same benchmark scenarios, see Refs. [30, 39, 40]. Here we compare those results with `MAPP1`, `MAPP2`, and `ANUBIS` for neutralino masses of 1200 MeV and 3000 MeV in the respective benchmark scenarios. We consider both a model-dependent $\lambda'_D/m^2_{\tilde{f}}$ vs. $\lambda'_P/m^2_{\tilde{f}}$ and the model-independent Br vs. $c\tau$ representation.

Firstly, we look at the model-dependent representa-

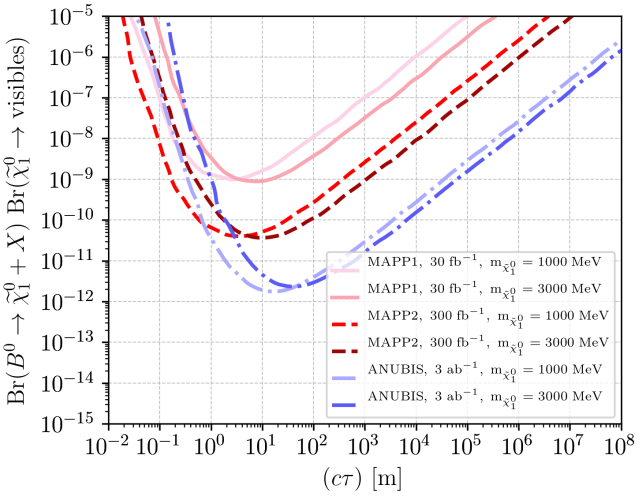


FIG. 6. Sensitivity estimate for a neutral long-lived fermion in a model-independent description for the charmed benchmark scenario 2 using our neutralino estimates. Labeling is similar to Fig. 4. For benchmark scenario 2 the considered neutralino masses are 1 and 3 GeV.

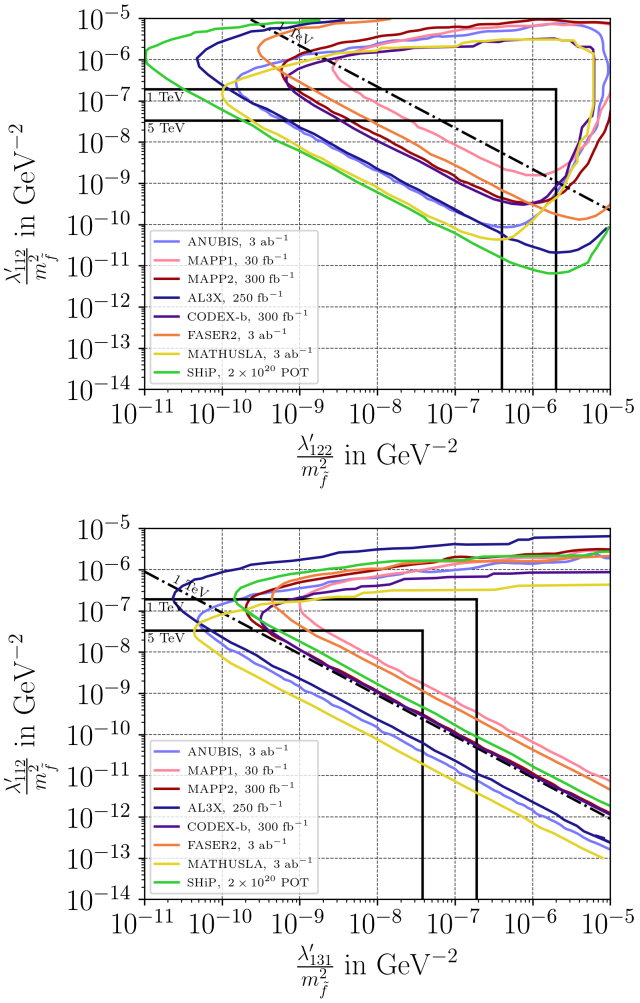


FIG. 7. Comparison of model-dependent numerical results. The top figure is for benchmark scenario 1, Tab. II for $m_{\tilde{\chi}_1^0} = 1200$ MeV, the lower for benchmark scenario 2, Tab. IV for $m_{\tilde{\chi}_1^0} = 3000$ MeV.

tion in Fig. 7. Benchmark scenario 1, Tab. II, is shown in the top figure, benchmark scenario 2, Tab. IV, in the lower. For both scenarios MAPP1 has the lowest reach while MAPP2 can substantially extend that reach to parameter regions comparable to other detectors, namely CODEX-B, FASER2 in the charmed scenario, and SHiP in the bottom meson scenario. The advantage of MAPP1 is, that the detector is already approved to be implemented for the LHC Run-3. The proximity to the ATLAS interaction point combined with the high integrated luminosity of $3\,\mathrm{ab}^{-1}$, however, propels ANUBIS to be the most promising proposed detector from this consideration. Only AL3X and MATHUSLA in both scenarios, and SHiP for the first scenario, can extend the existing sensitivity reach by a similar amount.

The model-independent representation is shown in Fig. 8. Again, benchmark scenario 1, is shown in the top figure, benchmark scenario 2 in the lower. For the first scenario, summarized in Tab. II, a hash grid is added in the upper right corner, *i.e.* for large $c\tau$ combined with a large product of branching ratios. This region is theoretically excluded and can not be probed in this scenario. The reason is the following. In order to continue the curves into the upper right, one must increase both the product of production branching ratios and the decay length. If one increases the production coupling $\lambda'_P = \lambda'_{122}$, then in the charmed scenario this also induces additional invisible decays, *cf.* Tab. II, which *reduces* the decay length. This can be compensated by decreasing the decay coupling $\lambda'_D = \lambda'_{112}$. But first of all this also reduces the product of production branching. Thus the increase in λ'_P must be larger than the decrease in λ'_D. At some point λ'_P dominates the decay length computation and the reduction in $c\tau$ can no longer be compensated by reducing λ'_D.

As before, compared to the other proposed experiments, MAPP1 has the lowest sensitivity reach for both scenarios because of its smaller angular coverage and lower integrated luminosity. However, MAPP1 is one of the few proposed far-detector programs that have been approved at CERN. MAPP2 extends the sensitivity reach in both directions. ANUBIS shows a similar behavior to MATHUSLA and is very promising to extend the reach for detecting any general long-lived particle.

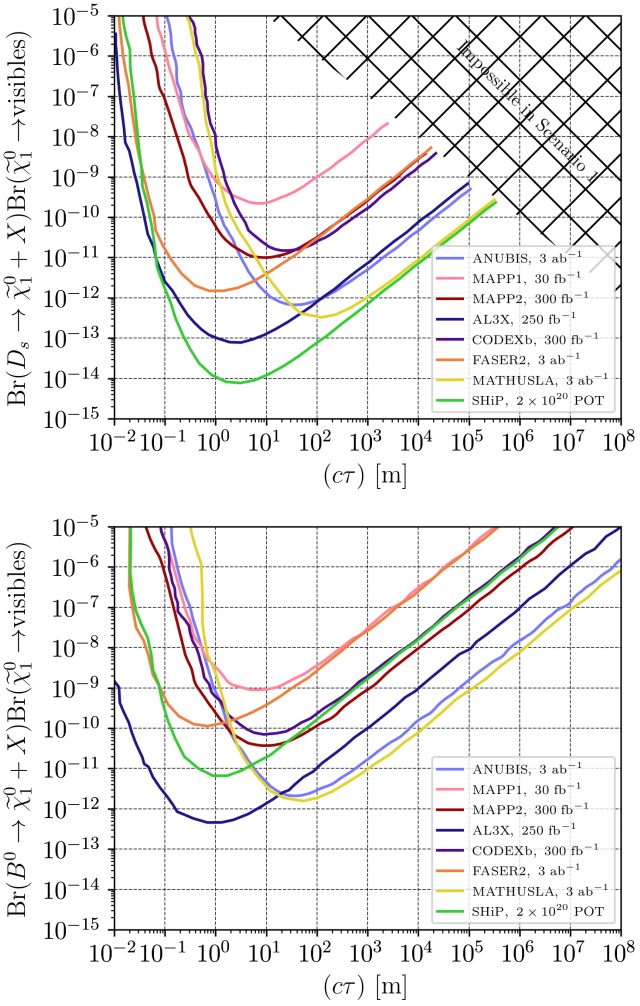


FIG. 8. Comparison of Br vs. $c\tau$ numerical results for various proposed detectors. The top figure is for benchmark scenario 1, *cf.* Tab. II, for $m_{\widetilde{\chi}_1^0} = 1200$ MeV, the lower for benchmark scenario 2, *cf.* Tab. IV, for $m_{\widetilde{\chi}_1^0} = 3000$ MeV. For the charmed scenario the region for large branching ratio products and large $c\tau$ is theoretically excluded. This region is marked by the hashed region.

V. CONCLUSIONS

In this paper we have investigated the potential of the experiments ANUBIS, MAPP1, and MAPP2 for the detection of long-lived light supersymmetric neutralinos produced via rare meson decays. This is an extension of previous works for the same model at other present and proposed experiments: ATLAS, SHiP, FASER, CODEX-b, MATHUSLA, and AL3X [30, 39, 40]. The neutralino decays via R-parity violating couplings to a lighter meson and a charged lepton. Following Refs. [30, 39], we consider two benchmark scenarios related to either charm or bottom mesons decays into the light neutralino.

We find that MAPP1 can strengthen current bounds on RPV-couplings in the charmed benchmark scenario. Its planned upgrade program MAPP2 may extend the sensitivity reach by one order of magnitude in $\lambda'/m_{\tilde{f}}^2$ compared to MAPP1, as a result of a greater integrated luminosity and increased solid-angle coverage. The sensitivity range of ANUBIS is shown to be the largest among the three detectors in both scenarios.

We compared the exclusion limits of these detectors to those of other experiments derived in Refs. [30, 39, 40]. MAPP1 is approved and will explore the parameter space. MAPP2 can go beyond this by more than an order of magnitude, and ANUBIS by yet another order of magnitude in Br, the product of production and decay branching ratios, reaching about 7×10^{-13}. But the potentially most sensitive experiment here is SHiP, followed by AL3X and MATHUSLA. See Fig. 8.

In the bottom scenario MAPP1 goes down to about 2×10^{-10} in Br, and MAPP2 extends this by more than an order of magnitude. Again ANUBIS can extend this by more than another order of magnitude reaching values as low as Br $\sim 3 \times 10^{-12}$. Here SHiP suffers from the lower production of B-mesons and the most sensitive proposed experiment is AL3X, followed by MATHUSLA and almost identically ANUBIS. In particular, AL3X can achieve this with an integrated luminosity more than one order of magnitude lower than that of MATHUSLA and ANUBIS, see Fig. 8.

Acknowledgements

We thank Vasiliki Mitsou for useful discussions. The work of H. K. D. was supported through the BMBF-Project 05H18PDCA1. Z. S. W. is supported partly by the Ministry of Science and Technology (MoST) of Taiwan with grant number MoST-109-2811-M-007-509, and partly by the Ministry of Science, ICT & Future Planning of Korea, the Pohang City Government, and the Gyeongsangbuk-do Provincial Government through the Young Scientist Training Asia Pacific Economic Cooperation program of the Asia Pacific Center for Theoretical Physics.

[1] J. Alimena *et al.*, (2019), arXiv:1903.04497.

[2] L. Lee, C. Ohm, A. Soffer, and T.-T. Yu, Prog. Part.

Nucl. Phys. **106**, 210 (2019), arXiv:1810.12602.
[3] D. Curtin *et al.*, Rept. Prog. Phys. **82**, 116201 (2019), arXiv:1806.07396.
[4] D. Choudhury and S. Sarkar, Phys. Lett. B **374**, 87 (1996), arXiv:hep-ph/9511357.
[5] D. Choudhury, H. K. Dreiner, P. Richardson, and S. Sarkar, Phys. Rev. D **61**, 095009 (2000), arXiv:hep-ph/9911365.
[6] G. Belanger, F. Boudjema, A. Pukhov, and S. Rosier-Lees, A Lower limit on the neutralino mass in the MSSM with nonuniversal gaugino masses, in *10th International Conference on Supersymmetry and Unification of Fundamental Interactions (SUSY02)*, pp. 919–924, 2002, arXiv:hep-ph/0212227.
[7] D. Hooper and T. Plehn, Phys. Lett. B **562**, 18 (2003), arXiv:hep-ph/0212226.
[8] A. Bottino, N. Fornengo, and S. Scopel, Phys. Rev. D **67**, 063519 (2003), arXiv:hep-ph/0212379.
[9] G. Belanger, F. Boudjema, A. Cottrant, A. Pukhov, and S. Rosier-Lees, JHEP **03**, 012 (2004), arXiv:hep-ph/0310037.
[10] D. Albornoz Vasquez, G. Belanger, C. Boehm, A. Pukhov, and J. Silk, Phys. Rev. D **82**, 115027 (2010), arXiv:1009.4380.
[11] L. Calibbi, J. M. Lindert, T. Ota, and Y. Takanishi, JHEP **10**, 132 (2013), arXiv:1307.4119.
[12] I. Gogoladze, J. D. Lykken, C. Macesanu, and S. Nandi, Phys. Rev. D **68**, 073004 (2003), arXiv:hep-ph/0211391.
[13] H. K. Dreiner *et al.*, Eur. Phys. J. C **62**, 547 (2009), arXiv:0901.3485.
[14] J. Grifols, E. Masso, and S. Peris, Phys. Lett. B **220**, 591 (1989).
[15] J. R. Ellis, K. A. Olive, S. Sarkar, and D. Sciama, Phys. Lett. B **215**, 404 (1988).
[16] K. Lau, Phys. Rev. D **47**, 1087 (1993).
[17] H. Dreiner, C. Hanhart, U. Langenfeld, and D. R. Phillips, Phys. Rev. D **68**, 055004 (2003), arXiv:hep-ph/0304289.
[18] H. K. Dreiner, J.-F. Fortin, J. Isern, and L. Ubaldi, Phys. Rev. D **88**, 043517 (2013), arXiv:1303.7232.
[19] S. Profumo, Phys. Rev. D **78**, 023507 (2008), arXiv:0806.2150.
[20] H. K. Dreiner, M. Hanussek, J. S. Kim, and S. Sarkar, Phys. Rev. D **85**, 065027 (2012), arXiv:1111.5715.
[21] P. Bechtle *et al.*, Eur. Phys. J. C **76**, 96 (2016), arXiv:1508.05951.
[22] H. K. Dreiner*An Introduction to explicit R-parity violation* Vol. 21 (, 2010), pp. 565–583, arXiv:hep-ph/9707435.
[23] R. Barbier *et al.*, Phys. Rept. **420**, 1 (2005), arXiv:hep-ph/0406039.
[24] R. N. Mohapatra*Supersymmetry and R-parity: an Overview* Vol. 90 (, 2015), p. 088004, arXiv:1503.06478.
[25] A. Dedes, H. K. Dreiner, and P. Richardson, Phys. Rev. D **65**, 015001 (2001), arXiv:hep-ph/0106199.
[26] H. Dreiner, G. Polesello, and M. Thormeier, (2002), arXiv:hep-ph/0207160.
[27] H. Dreiner *et al.*, Phys. Rev. D **80**, 035018 (2009), arXiv:0905.2051.
[28] S. Alekhin *et al.*, Rept. Prog. Phys. **79**, 124201 (2016), arXiv:1504.04855.
[29] D. Gorbunov and I. Timiryasov, Phys. Rev. D **92**, 075015 (2015), arXiv:1508.01780.
[30] J. de Vries, H. K. Dreiner, and D. Schmeier, Phys. Rev. D **94**, 035006 (2016), arXiv:1511.07436.
[31] V. V. Gligorov, S. Knapen, M. Papucci, and D. J. Robinson, Phys. Rev. D **97**, 015023 (2018), arXiv:1708.09395.
[32] G. Aielli *et al.*, (2019), arXiv:1911.00481.
[33] J. L. Feng, I. Galon, F. Kling, and S. Trojanowski, Phys. Rev. D **97**, 035001 (2018), arXiv:1708.09389.
[34] FASER, A. Ariga *et al.*, Phys. Rev. D **99**, 095011 (2019), arXiv:1811.12522.
[35] FASER, A. Ariga *et al.*, (2019), arXiv:1901.04468.
[36] J. P. Chou, D. Curtin, and H. Lubatti, Phys. Lett. B **767**, 29 (2017), arXiv:1606.06298.
[37] V. V. Gligorov, S. Knapen, B. Nachman, M. Papucci, and D. J. Robinson, Phys. Rev. D **99**, 015023 (2019), arXiv:1810.03636.
[38] J. C. Helo, M. Hirsch, and Z. S. Wang, JHEP **07**, 056 (2018), arXiv:1803.02212.
[39] D. Dercks, J. De Vries, H. K. Dreiner, and Z. S. Wang, Phys. Rev. D **99**, 055039 (2019), arXiv:1810.03617.
[40] D. Dercks, H. K. Dreiner, M. Hirsch, and Z. S. Wang, Phys. Rev. D **99**, 055020 (2019), arXiv:1811.01995.
[41] Z. S. Wang and K. Wang, Phys. Rev. D **101**, 115018 (2020), arXiv:1904.10661.
[42] Z. S. Wang and K. Wang, Phys. Rev. D **101**, 075046 (2020), arXiv:1911.06576.
[43] CMS, A. M. Sirunyan *et al.*, Phys. Lett. B **797**, 134876 (2019), arXiv:1906.06441.
[44] ATLAS, G. Aad *et al.*, Phys. Rev. D **101**, 052013 (2020), arXiv:1911.12575.
[45] M. Bauer, O. Brandt, L. Lee, and C. Ohm, (2019), arXiv:1909.13022.
[46] M. Hirsch and Z. S. Wang, Phys. Rev. D **101**, 055034 (2020), arXiv:2001.04750.
[47] MoEDAL, M. Staelens, Recent Results and Future Plans of the MoEDAL Experiment, in *Meeting of the Division of Particles and Fields of the American Physical Society*, 2019, arXiv:1910.05772.
[48] A. Bartl, W. Majerotto, and N. Oshimo, Phys. Lett. B **216**, 233 (1989).
[49] B. Allanach, A. Dedes, and H. Dreiner, Phys. Rev. D **69**, 115002 (2004), arXiv:hep-ph/0309196, [Erratum: Phys.Rev.D 72, 079902 (2005)].
[50] L. E. Ibanez and G. G. Ross, Nucl. Phys. B **368**, 3 (1992).
[51] H. K. Dreiner, M. Hanussek, and C. Luhn, Phys. Rev. D **86**, 055012 (2012), arXiv:1206.6305.
[52] H. K. Dreiner and S. Grab, Phys. Lett. B **679**, 45 (2009), arXiv:0811.0200.
[53] D. Dercks, H. Dreiner, M. E. Krauss, T. Opferkuch,

and A. Reinert, Eur. Phys. J. C **77**, 856 (2017), arXiv:1706.09418.

[54] B. Allanach, A. Dedes, and H. K. Dreiner, Phys. Rev. D **60**, 056002 (1999), arXiv:hep-ph/9902251, [Erratum: Phys.Rev.D 86, 039906 (2012)].

[55] B. Allanach, A. Dedes, and H. K. Dreiner, Phys. Rev. D **60**, 075014 (1999), arXiv:hep-ph/9906209.

[56] V. D. Barger, G. Giudice, and T. Han, Phys. Rev. D **40**, 2987 (1989).

[57] G. Bhattacharyya, A Brief review of R-parity violating couplings, in *Workshop on Physics Beyond the Standard Model: Beyond the Desert: Accelerator and Nonaccelerator Approaches*, pp. 194–201, 1997, arXiv:hep-ph/9709395.

[58] Y. Kao and T. Takeuchi, (2009), arXiv:0910.4980.

[59] F. Domingo *et al.*, JHEP **02**, 066 (2019), arXiv:1810.08228.

[60] S. Bansal, A. Delgado, C. Kolda, and M. Quiros, Phys. Rev. D **100**, 093005 (2019), arXiv:1906.01063.

[61] [ATLAS], ATLAS-CONF-2015-018.

[62] V. Khachatryan *et al.* [CMS], Phys. Lett. B **760** (2016), 178-201 doi:10.1016/j.physletb.2016.06.039 [arXiv:1602.04334 [hep-ex]].

[63] LHCb, R. Aaij *et al.*, JHEP **03**, 159 (2016), arXiv:1510.01707, [Erratum: JHEP 09, 013 (2016), Erratum: JHEP 05, 074 (2017)].

[64] LHCb, R. Aaij *et al.*, Phys. Rev. Lett. **118**, 052002 (2017), arXiv:1612.05140, [Erratum: Phys.Rev.Lett. 119, 169901 (2017)].

[65] M. Cacciari, M. Greco, and P. Nason, JHEP **05**, 007 (1998), arXiv:hep-ph/9803400.

[66] M. Cacciari, S. Frixione, and P. Nason, JHEP **03**, 006 (2001), arXiv:hep-ph/0102134.

[67] M. Cacciari *et al.*, JHEP **10**, 137 (2012), arXiv:1205.6344.

[68] M. Cacciari, M. L. Mangano, and P. Nason, Eur. Phys. J. C **75**, 610 (2015), arXiv:1507.06197.

[69] T. Sjostrand, S. Mrenna, and P. Z. Skands, Comput. Phys. Commun. **178**, 852 (2008), arXiv:0710.3820.

[70] T. Sjostrand, S. Mrenna, and P. Z. Skands, JHEP **05**, 026 (2006), arXiv:hep-ph/0603175.